Numerical simulation analysis of heat and mass transfer of saline wastewater in a falling film evaporation tube based on different inlet modes

Xiang Cheng Kong[a], You Le Liu[b], Hua Shan Li[a], Jian Liang Xue [a,d], Bing Liu[e], Dong Le Cheng [a,c,d,*], Yu Gao[a,d] and Xin Feng Xiao[a,d]

[a] College of Safety and Environmental Engineering, Shandong University of Science and Technology, Qingdao, Shandong 266590, China
[b] China University of Mining and Technology, Xuzhou, Jiangsu 221116, China
[c] Centre for Technology in Water and Wastewater, School of Civil and Environmental Engineering, University of Technology Sydney, Sydney, NSW 2007, Australia
[d] Institute of Yellow River Delta Earth Surface Processes and Ecological Integrity, Shandong University of Science and Technology, Qingdao, Shandong 266590, China
[e] College of Mechanical and Electronic Engineering, Shandong University of Science and Technology, Qingdao, Shandong 266590, China
*Corresponding author. E-mail: donglelecheng@gmail.com

JLX, 0000-0002-7066-8351; DLC, 0000-0001-9010-8274

ABSTRACT

Falling film evaporation technology is widely used in the treatment of salt-containing wastewater in coal chemical industry. However, there is still a lack of research on the inlet method of vertical falling film evaporation tubes. In this paper, the heat and mass transfer processes of saline wastewater under vertical and tangential inlets were investigated using numerical simulations. On this basis, the differences in flow and heat transfer processes between saline wastewater and pure water under tangential inlet were investigated. The results showed that the flow velocity of saline wastewater with a falling film evaporation tube in a tangential inlet mode was larger. Meanwhile, the turbulence in this way was more intense and the fluid temperature in the vertical tube was higher. Saline wastewater has higher temperature and smaller liquid volume fraction than pure water liquid membrane in the range of 193–1,000 mm from the inlet. The use of tangential inlet method to treat salt-containing wastewater has higher evaporation efficiency and is a very effective way to guide the improvement of heat transfer efficiency.

Key words: saline wastewater, pure water, falling film evaporation, vertical tube, mass and heat transfer

HIGHLIGHTS

- Study on the heat transfer of a falling film evaporator tube with different inlets.
- The liquid film velocity at the tangential inlet is faster than that at the vertical inlet.
- Salty wastewater is thinner than pure water, which is more conducive to evaporation.

GRAPHICAL ABSTRACT
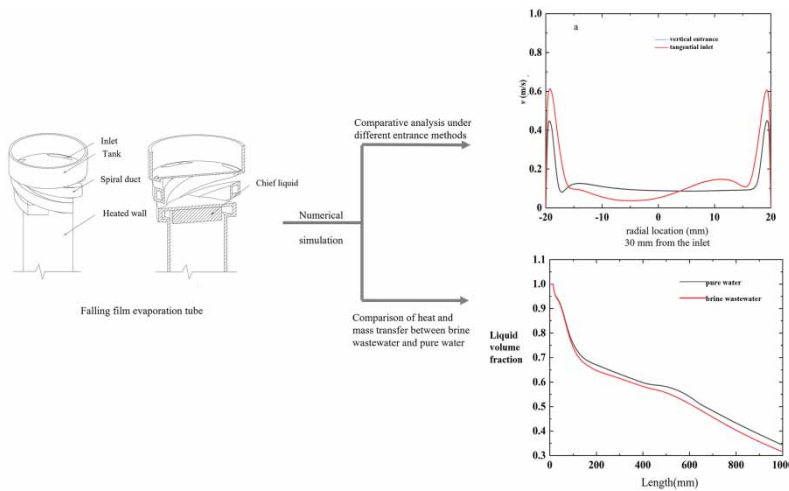
1. INTRODUCTION

In recent years, oil, gas, and coal chemical industries have been widely used in human production and life (Lefebvre & Moletta 2006). These industries not only require a large amount of domestic water in the process of utilization and development, but also discharge many industrial wastewater that cannot be directly used. With the continuous increase of people's water consumption, the problem of how to realize the development and utilization of wastewater has plagued the further development of the world economy (Zhang *et al.* 2002). Salt-containing wastewater has been widely studied by its high discharge, difficult treatment, and complex composition. It is important to carry out basic research on the resourceful and efficient utilization of saline wastewater to effectively enhance the utilization value of wastewater and achieve 'zero discharge' of wastewater (Dolatabadi *et al.* 2021).

At present, there are many treatment methods for saline wastewater, including biochemical method (Zhao *et al.* 2017), gas fluidized bed method (Shi *et al.* 2020), and thermal treatment method (Ng *et al.* 2015; Lappalainen *et al.* 2017; Zhou *et al.* 2019). Among these methods, the thermal treatment method can take advantage of the difference in solubility of the components of the mixture in the same solvent or the significant difference in solubility between hot and cold conditions, while the crystallization method is used for separation (Liu *et al.* 2020; Bing *et al.* 2021). It is also widely used in the treatment of salt-containing wastewater because of its obvious advantages such as small footprint, high heat transfer coefficient, and more stable performance (Al-Sahali & Ettouney 2007). The falling film evaporator has been widely studied as the core heating device of the thermal treatment method.

To improve the evaporation effect and evaporation efficiency, the role of various factors on the mass and heat transfer is generally studied by simulating in a falling film evaporation tube. For this reason, many scholars have conducted more systematic research on vertical falling film evaporation tubes. The process of studying evaporation needs to be supported by adequate theory. Zhang *et al.* (2015) and Tian *et al.* (2018) conducted a numerical simulation and experimental study of the heat transfer mechanism of pure water in a saturated pool using a computational fluid dynamics (CFD) model. Gommed *et al.* (2001) developed a prediction tool that can predict the heat and mass transfer during the absorption of ammonia vapor into the liquid layer inside a vertical tube. Also, it is necessary to study the microscopic flow in the falling film evaporation tube. Oubella *et al.* (2015) performed a numerical study of mixed convective heat and mass transfer during evaporation, which can play an important role in improving the evaporation efficiency of liquids in evaporation tubes. These scholars' studies on vertical tubes are based on the heat and mass transfer of evaporation tubes under the vertical inlet method, and the heat transfer efficiency does not change much. To obtain higher heat transfer efficiency, changing the inlet method is one of the ways to improve efficiency.

Wang *et al.* (2020) used the volume of fluid (VOF) model to numerically simulate the flow characteristics of pure water in vapor–liquid two-phase counterflow under different structural conditions, and obtained the effects of tube length, tube diameter, and annular cloth spacing on membrane distribution and membrane fluctuations. Li *et al.* (2017) investigated the evaporative mass

transfer characteristics of a falling water film under counterflow laminar conditions, reviewed previous studies on heat transfer in water film flow and expressed these factors in a comprehensive manner, and then conducted an experimental study to reveal the characteristics of the local Sherwood number along the flow direction and determined the correlation between evaporative mass transfer. Compared to pure water, the physical parameters in brine have a greater impact on the performance of brine in evaporation (Cao *et al.* 2019). Therefore, there is a lack of research on the flow of brine in the evaporation tube.

To investigate the differences in heat and mass transfer in different inlet methods of falling film evaporation tubes. This paper studied the difference of various parameters between the simulated working conditions of wastewater entering the evaporation tube with the new tangential inlet method and the traditional inlet method in a vertical falling film evaporation tube. Also, on this basis, the differences in the physical properties of pure water and simulated working wastewater under the new tangential inlet method and the process of heat and mass transfer in the falling film evaporation tube were studied, providing a new direction for achieving high efficiency evaporation.

2. NUMERICAL SIMULATION METHOD

2.1. Physical mode

The physical model of the vertical pipe used in this study is shown in Figure 1. There is a liquid storage tank above the vertical pipe in Figure 1(a). To reduce the kinetic energy loss of the salt-containing wastewater during the flow process, four spiral conduits are connected below the vertical pipe. The salt-containing wastewater to be evaporated enters the liquid storage tank from the inlet and is affected by gravity It flows down to the liquid distributor in Figure 1(b), and the salty wastewater is evenly distributed into the vertical falling film evaporation tube through the liquid distributor.

2.2. Mathematical models

CFD as a comprehensive tool has been validated over the past few years to elucidate the details of flow patterns. In this study, the saline wastewater flows in the form of a liquid film in the vertical pipe, and heat transfer is involved. The liquid film flow and the generated steam belong to the two-phase stratified flow of vapor and liquid. Considering the complexity and numerical value of the flow and heat transfer process. Therefore, the VOF model was also used to numerically simulate the falling film flow in this study. In the VOF model, the volume fraction of fluid phase α is defined, and in each control volume, the sum of volume fraction α_b of different phases is 1:

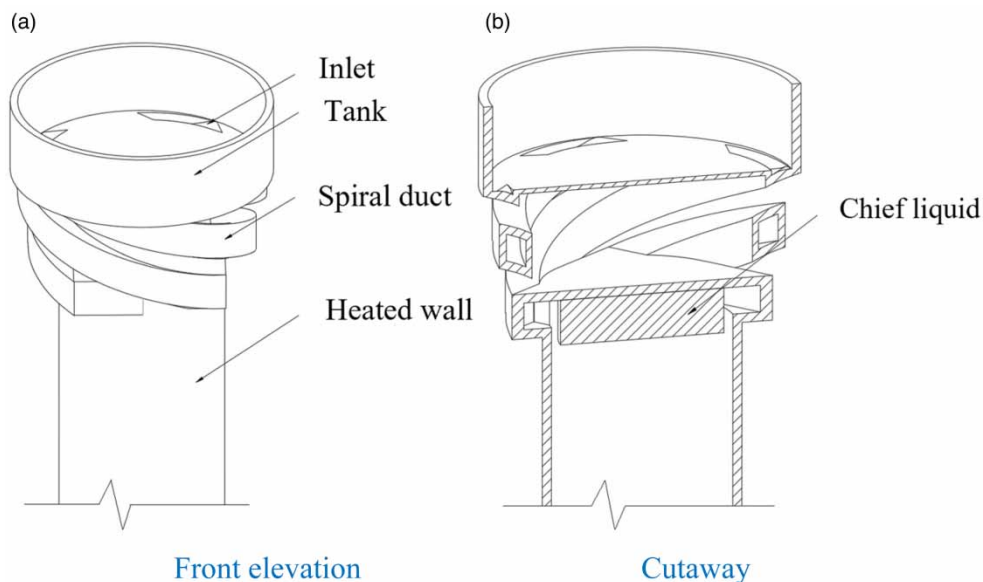$$\sum_{k=1}^{n} \alpha_b = 1 \tag{1}$$

Figure 1 | Physical model: (a) front elevation and (b) cutaway.

where $n = 2$, b is the liquid phase (or gas phase), and the sum of the two gas volume fractions is 1. The viscosity μ and density ρ of each control body can be derived from the following two equations:

$$\rho = \alpha_L \rho_L + (1 - \alpha_L)\rho_G \tag{2}$$

$$\mu = \alpha_L \mu_L + (1 - \alpha_L)\mu_G \tag{3}$$

Then, the continuity equation can be described as follows:

$$\frac{\partial \rho}{\partial t} + \nabla \cdot (\rho \vec{u}) = S_i \tag{4}$$

where ρ is the density of the fluid, $\vec{u}$ and t are the velocity vector and time. There is no phase change during the cold film formation process, so the default mass source term S_i is zero. However, S_i is the mass transfer source term in the evaporation process (gas–liquid mass transfer occurs in both).

Each control body has the same velocity field in both phases. Also, the momentum equation can be expressed as follows:

$$\frac{\partial}{\partial t}(\rho \vec{u}) + \nabla \cdot (\rho \vec{u}\vec{u}) = -\nabla p + \nabla \cdot [\mu(\nabla \vec{u} + \vec{u}^T)] + \rho \vec{g} + F \tag{5}$$

where $p, \mu, T, \vec{g}$, and F are the pressure, the viscosity, the temperature, the acceleration of gravity, and the volume force source term, respectively.

The energy equation may be written as follows:

$$\frac{\partial}{\partial t}(\rho E) + \nabla(\vec{u}(\rho E + p)) = \nabla(k_{eff} \nabla T) + Q \tag{6}$$

where E, k_{eff}, and Q are the energy, the effective heat transfer coefficient, and the source term of fluid, respectively.

The RNG k–ε model is selected as the turbulence model according to the working mass conditions and the characteristics of the high-flow descending film in the tube.

$$\mu_t = C_\mu \rho \frac{k}{\varepsilon^2} \tag{7}$$

The turbulent viscosity μ_t is correlated with the turbulent energy k and the dissipation rate of turbulence ε.

The turbulent energy equation k is as follows:

$$\frac{\partial(\rho k)}{\partial t} + \frac{\partial(\rho k \mu_i)}{\partial x_i} = \frac{\partial}{\partial x_j}\left[(\alpha_k \mu_{\text{eff}})\frac{\partial k}{\partial x_j}\right] + G_k + G_b - \rho \varepsilon - Y_M + S \tag{8}$$

where α_k and μ_{eff} are the turbulent Prandtl number and the effective viscosity. G_k is the turbulent kinetic energy generated by the laminar velocity. G_b, ε, Y_M are the turbulent kinetic energy generated by buoyancy, the dissipation rate of turbulent kinetic energy, and the wave generated by the transition diffusion in compressible turbulence, respectively.

The turbulent dissipation rate equation ε is as follows:

$$\frac{\partial(\rho \varepsilon)}{\partial t} + \frac{\partial(\rho \varepsilon \mu_i)}{\partial x_i} = \frac{\partial}{\partial x_j}\left[(\alpha_\varepsilon \mu_{\text{eff}})\frac{\partial \varepsilon}{\partial x_j}\right] + C_{1\varepsilon}\frac{\varepsilon}{k}(G_k + C_{3\varepsilon}G_b) - C_{2\varepsilon}\rho\frac{\varepsilon^2}{k} - R \tag{9}$$

where $C_{1\varepsilon}$, $C_{2\varepsilon}$, and $C_{3\varepsilon}$ are the constants. R is a user-defined parameter.

The convective coefficient of heat transmission of the liquid film can be derived from the Newtonian cooling equation:

$$h = \frac{q_w}{\Delta T} = \frac{q_w}{T_w - T_m} \tag{10}$$

where T_w, T_m, and q_w are the wall temperature, the average temperature of the liquid film, and the heat flux density, respectively.

The heat flux is derived from the following equation:

$$q_w = \frac{Q_L}{\pi D_1 L_1} \tag{11}$$

where Q_L is the heat flow rate.

2.3. Setting boundary and initial conditions

The settings of the boundary and initial conditions are shown in Table 1. In addition, heat walls are defined as constant temperature, no-slip, no penetration, and zero thickness, while other walls are defined as no-slip, no penetration, and insulation.

2.4. Assumptions

This paper simulates a falling film outside the tube and vapor inside the tube. The results of the study help to better understand the heat flow process of the falling film evaporator. The following are the hypotheses of this paper:

- The fluid is continuous, incompressible, and has constant physical properties.
- The vertical tube wall is completely wetted by the fluid, so the contact angle is 0 degrees.
- The operating conditions are adiabatic.
- There is no pressure difference in the simulation domain.
- The effect of vapor velocity on the descending film is negligible.

2.5. Mesh independence tests

High-quality meshing is the foundation of numerical simulation research because it is related to the accuracy of the simulation. The fluid domain structure grid of the tangential inlet vertical pipe in this study is shown in Figure 2(a). To obtain a higher quality mesh, the main part is divided into an O-shape to obtain a higher quality mesh, and the boundary mesh of the evaporation tube is refined, so that more accurate boundary features can be obtained.

To avoid the calculation error caused by the grid accuracy problem, grid-independent detection was performed. Seven groups of meshes with total mesh numbers from 94,986 to 1,628,483 were used and the film thicknesses at the middle of the evaporation tube were compared, and the simulation results are shown in Figure 2(b), where the calculated results increase with the number of mesh divisions. However, when exceeding 500,000, the results show only a slight difference. To save time and computational resources, a total of 505,216 mesh numbers were selected.

3. RESULTS AND DISCUSSION

3.1. Comparative analysis of flow field characteristics in a vertical tube with tangential and vertical inlets

The fluid flow velocity, turbulence intensity, and fluid temperature of the saline wastewater in the evaporation tube are changed for both vertical and tangential inlet methods (Fang et al. 2019). In this section, the vertical inlet method and tangential

Table 1 | Boundary conditions and solver parameters

Boundary conditions/solver	Setting
Multiphase	Volume of fluid
Viscous	RNG $k - \varepsilon$
Discretization scheme of pressure	PRESTO!
Pressure–velocity coupling	SIMPLE
Discretization scheme of volume fraction	QUICK
Discretization scheme of momentum	QUICK
Discretization scheme of energy	QUICK

(a)

Fluid domain structure grid

(b)

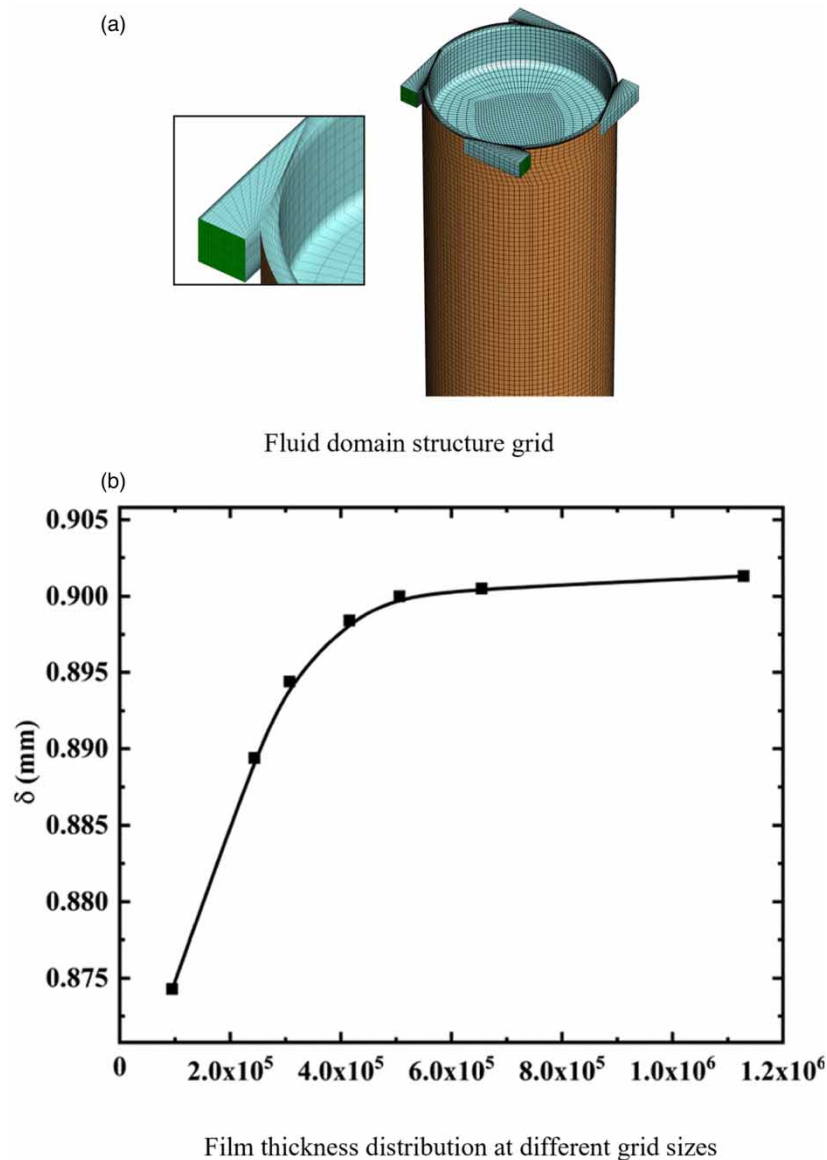Film thickness distribution at different grid sizes

Figure 2 | Mesh distribution and independence test.

inlet method of the vertical pipe are investigated using salt-containing wastewater (2% NaCl). The variation of thermodynamic parameters of saline wastewater in vertical tubes at 30, 100, 150, and 200 mm from the inlet was highlighted for comparison.

The conditions for the numerical simulation in this section are as follows: inlet temperature of 313 K, heating temperature of 383 K, and spray density of 0.49 kg/(m·s).

3.1.1. Speed distribution

Figure 3 shows the radial distribution of velocity magnitude at different axial positions of the vertical inlet and tangential inlet vertical tubes.

The results show that the fluid velocity in the vertical tube with tangential inlet is larger. Under the same conditions of inlet flow rate, the higher the velocity in the liquid phase region, the higher the turbulence intensity and the better the heat transfer effect. In the vapor phase region, especially at the vapor–liquid interface, larger vapor velocities are also beneficial for convective heat transfer and liquid film evaporation processes here.
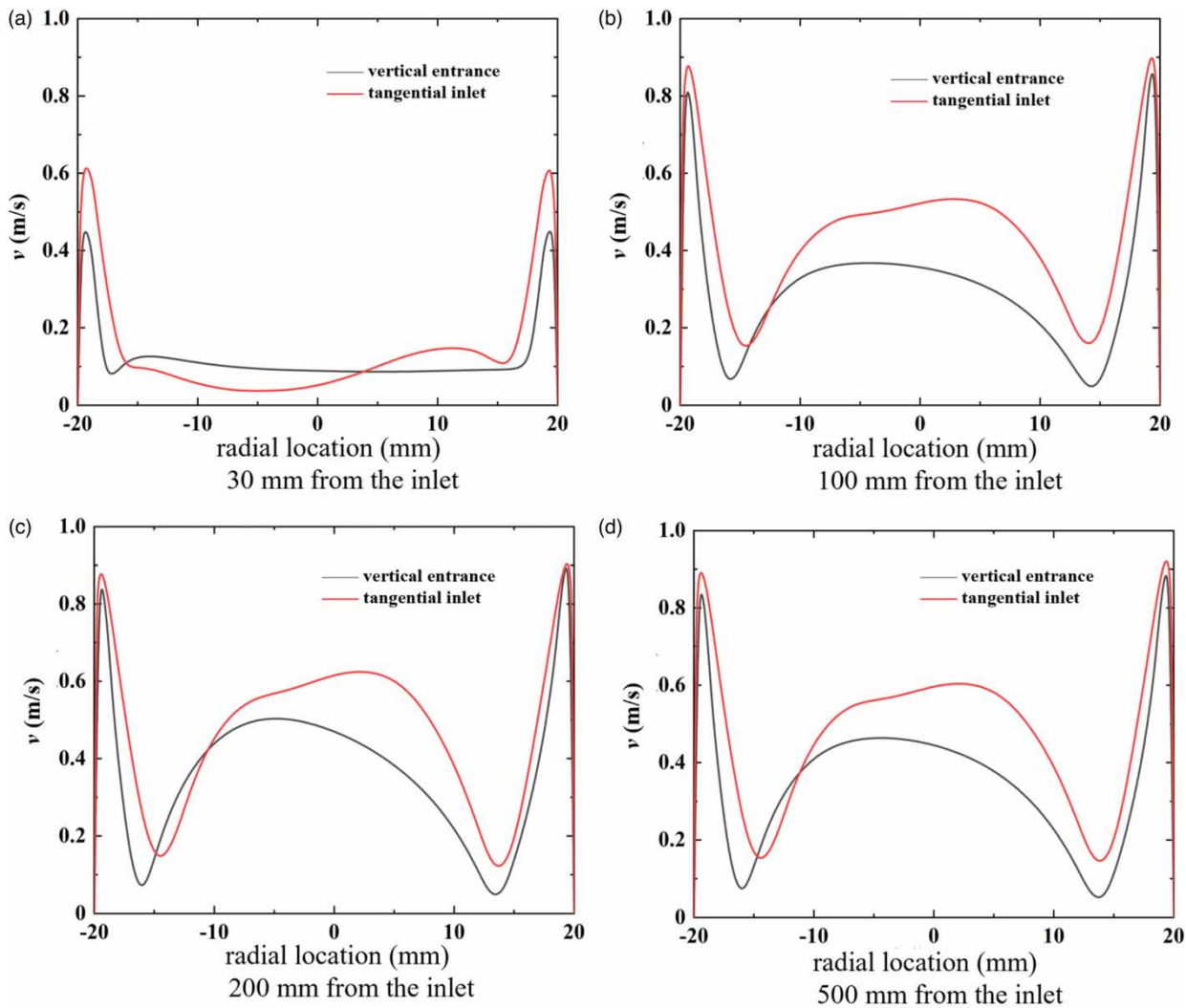
Figure 3 | Distribution of radial velocity at different axial positions.

As shown in Figure 3(a), the magnitude of fluid velocity in the vertical tube fluctuates widely in the tangential inlet method due to different designs. The fluid velocity of the vertical tube with tangential inlet is large, especially in the liquid film area, where the maximum difference in liquid film velocity is around 0.16 m/s.

In addition, as shown in Figure 3(b), the overall fluid velocity of the vertical tube with a tangential inlet is greater than that of the vertical inlet vertical tube here due to the difference in the initial velocity into the evaporation tube. The maximum velocity difference in the liquid film area is around 0.08 m/s, and the maximum difference in the velocity size in the vapor phase area is around 0.21 m/s.

Compared to Figure 3(b) in Figure 3(c), the difference in fluid velocity magnitude decreases in the liquid film region near the tube wall, while the difference is larger in the vapor phase region at the center of the tube. In the liquid film area, the difference of the inlet method has a small effect on the liquid film velocity, the magnitude of which ranges from 0.84 to 0.9 m/s. While in the vapor phase region, the maximum difference in fluid velocity magnitude is around 0.2 m/s, with the maximum fluid velocity in the center of the tube.

Combined with Figure 7(c), it can be obtained that in Figure 3(d), the fluid velocity variation in the vertical tube by gravity and other influences basically tends to be stable (Mura & Gourdon 2016). The velocity in the liquid film region of the vertical tube with tangential inlet is about 0.5 m/s higher than that of the vertical inlet; the velocity of the fluid in the vapor phase region is basically constant.

3.1.2. Turbulence strength distribution

Figure 4 shows the radial distribution of turbulence intensity magnitudes at different axial positions of the vertical inlet and tangential inlet vertical tubes. Compared with the vertical tube with vertical inlet, the intensity of fluid turbulence in the vertical tube with tangential inlet, especially at the vapor–liquid interface, is higher, which undoubtedly facilitates the evaporation process of liquid film.

As shown in Figure 4(a), the fluid turbulence intensity in the vertical tube with tangential inlet, especially at the vapor–liquid interface, is about 5% higher than that in the vertical inlet vertical tube. The turbulent intensity of the fluid in the vertical tube in this region is relatively small overall, and in the liquid phase region, along the radial direction, the turbulent intensity of the liquid film increases relative to the wall distance and reaches a maximum at the vapor–liquid intersection. In the vapor phase region, the vapor phase turbulence intensity is more stable in the range of −15 to 15 mm from the tube mid-axis. In the radial direction, the turbulence intensity of the vapor phase increases with increasing distance from the center of the tube in the range of 15 mm from the center of the tube to the vapor–liquid interface.

From Figure 4(b), it can be seen that the turbulence intensity maximum is at the vapor–liquid interface and decreases along the radial direction from the vapor–liquid interface to both sides. In the liquid phase region, the reduction of the turbulence intensity of the liquid film is larger along the radial direction, while the reduction is smaller in the vapor phase region. The difference in the turbulence intensity of the liquid film in the liquid phase region is small when the inlet mode is different. While at the vapor–liquid interface, the turbulence intensity of the fluid in the vertical tube with a tangential inlet is larger with a maximum difference of about 3%.

The magnitude of turbulence intensity in these two cross-sections in Figure 4(c) and 4(d) is similar to the turbulence intensity distribution pattern in Figure 4(b). It is worth noting that the maximum values of fluid turbulence intensity in these two
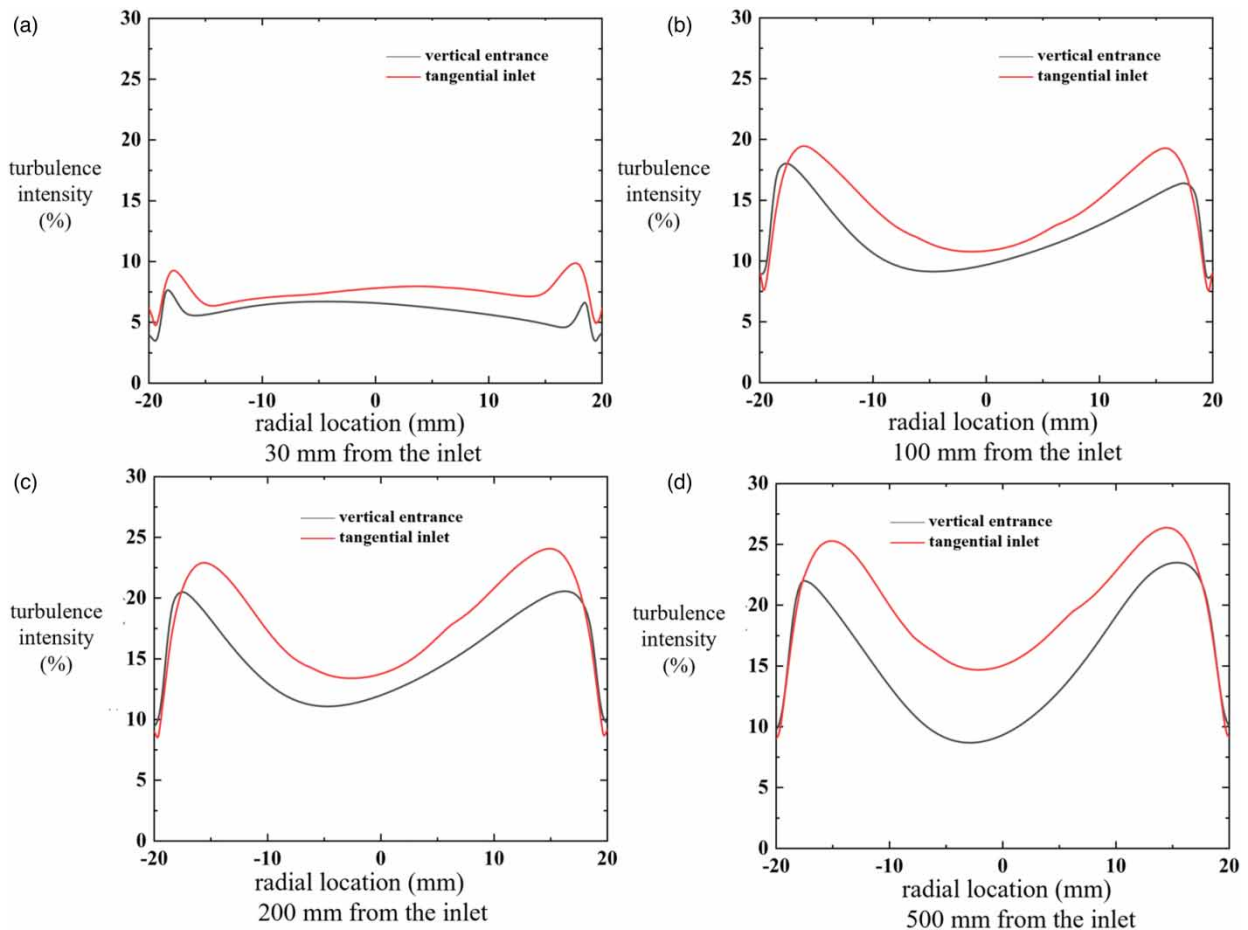

Figure 4 | Distribution of radial turbulence intensity at different axial positions.

cross-sections due to the flow velocity do not appear at the vapor–liquid interface, and the overall fluid turbulence intensity increases (Karimi & Kawaji 1999). The maximum value of turbulence intensity of the fluid reaches about 24% at Figure 4(c). While in Figure 4(d), the maximum turbulence intensity of the fluid in the vertical tube with tangential inlet reaches about 27%.

3.1.3. Distribution of temperature

Figure 5 compares and analyzes the temperature distribution in the radial section near the wall at different axial positions for different inlet methods.

From Figure 5(a) and 5(b), it can be seen that the temperature of the liquid film increases faster in this range and the temperature gradient of the radial section decreases. The main reason is that the initial temperature of the liquid film is low, the temperature of the tube wall is high, and the liquid film is fully heated after entering the evaporation tube. Since the liquid film is better buffered in the tangential inlet method, the temperature of the liquid film in the vertical tube with tangential inlet is higher and the temperature rise is large. The maximum difference in temperature between the two compared to the vertical inlet method is about 9 K.

The liquid film temperature in the vertical tube with different inlet methods in Figure 5(c) is elevated to more than 350 K. The temperature of the liquid film in the vertical tube with tangential inlet is higher, and the difference between the liquid film temperature and that in the vertical inlet vertical tube is about 5 K.
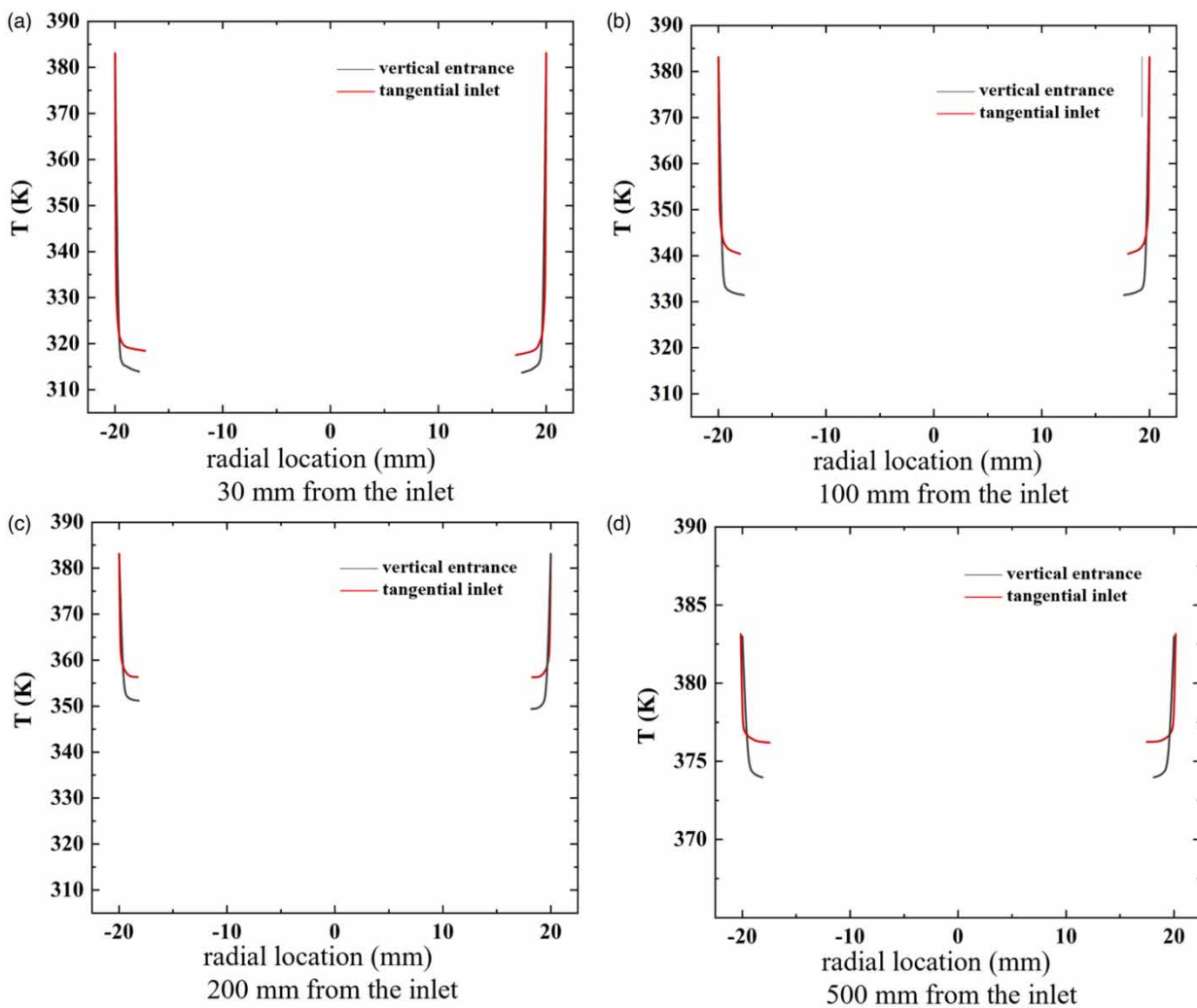

Figure 5 | Distribution of temperature at different axial positions.

As shown in Figure 5(d), the liquid film increases to a more stable value after a full development in the upper part of the vertical tube. Thereby this results in a smaller difference in fluid temperature in the vertical tubes of the two different inlet methods.

3.2. Comparison of heat and mass transfer between saline wastewater and pure water

To more accurately understand the flow and heat transfer characteristics of highly saline wastewater in a vertical tube, this section compares the physical parameters of pure water and saline wastewater. On this basis, the temperature distribution, liquid volume fraction distribution, and tangential velocity distribution of the two liquid films in the vertical tube were compared and analyzed.

First, numerical simulations of pure water and saline wastewater were carried out under the conditions of inlet water temperature $T_0 = 303$ K, isothermal wall temperature $T_w = 383$ K, and inlet water velocity $V_0 = 0.4$ m/s. In simulating the evaporation of saline wastewater by falling film, in order to avoid the problem of crystallization due to high salt concentration at the late stage of evaporation, 2% saline wastewater (the wastewater is mainly NaCl for example), this paper only considers the concentration process of saline wastewater in a vertical tube and focuses on the heat and mass transfer mechanism in this process. It is worth mentioning that the diameter of the evaporation tube for this simulation is 40 mm and the length is 1,000 mm.
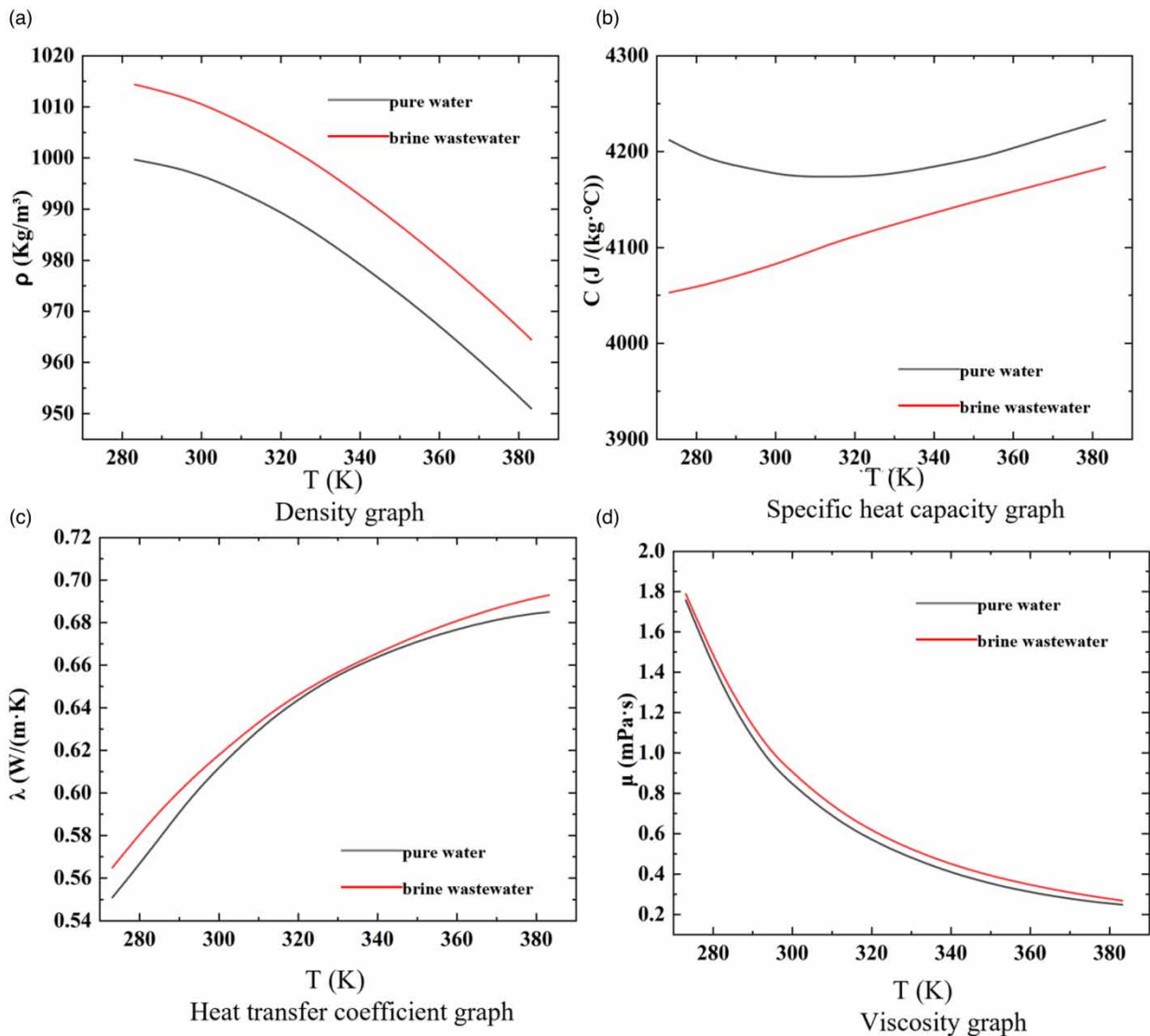

Figure 6 | Variations of physical parameters of saline wastewater and pure water with temperature.

3.2.1. Comparison of the variation of physical parameters of saline wastewater and pure water with temperature

The physical parameters of liquids change with temperature, and the physical parameters of different liquids will also be different. With the progress of the evaporation process, the temperature of the liquid in the vertical tube changes, which also has a certain influence on its physical parameters (Zezhong 2014). Figure 6 shows the changes of density, specific heat capacity, thermal conductivity, and viscosity of saline wastewater and pure water at different temperature conditions.

Figure 6(a) depicts the variation of the density of the two liquids with temperature. It can be seen that the density of the liquid decreases with the increase of temperature, and the density of the saline wastewater is slightly greater than that of pure water. Figure 6(b) shows the variation of specific heat capacity of the two liquids with temperature. From the figure, it can be seen that the specific heat capacity of saline wastewater increases with the increase of temperature, while the specific heat capacity of pure water decreases with the increase of temperature between 273 and 320 K and increases with the increase of temperature between 320 and 383 K. What's more, the specific heat capacity of pure water is slightly larger than that of saline wastewater. As can be seen in Figure 6(c), the thermal conductivity of the two liquids increases with the increase of temperature, and the thermal conductivity of saline wastewater is slightly larger than that of pure water. As shown in Figure 6(d), the viscosity of the two liquids decreased with the increase of temperature, but the viscosity of saline wastewater was slightly larger than that of pure water.

3.2.2. Temperature change of liquid film formed by saline wastewater and pure water in a vertical tube along the axial direction of the tube

Figure 7 shows the temperature variation along the axial direction of the liquid film formed in the vertical tube for saline wastewater and pure water. It can be seen from the figure that the difference between the temperature of the saline-containing wastewater liquid film and the pure water liquid film temperature is small within the range of 0–193 mm from the inlet, while the temperature of the salt-containing wastewater liquid film within the range of 193–1,000 mm from the inlet is slightly different which is higher than the temperature of the pure water film.

The reason for this situation is related to the specific heat capacity and thermal conductivity of both. Referring to Figure 6(b) and 6(c), it can be seen that the specific heat capacity of saline wastewater is smaller than that of pure water, and the thermal conductivity is greater.

3.2.3. Liquid volume fraction distribution of the liquid film formed by saline wastewater and pure water in a vertical tube

Figure 8 shows a distribution diagram of the liquid volume fraction of the liquid film formed in the vertical pipe of pure water and saline wastewater. It can be noticed that the liquid film liquid volume fraction of saline wastewater and pure water has the same trend of change, that is, the liquid volume fraction gradually decreases after entering the vertical pipe and reaches a
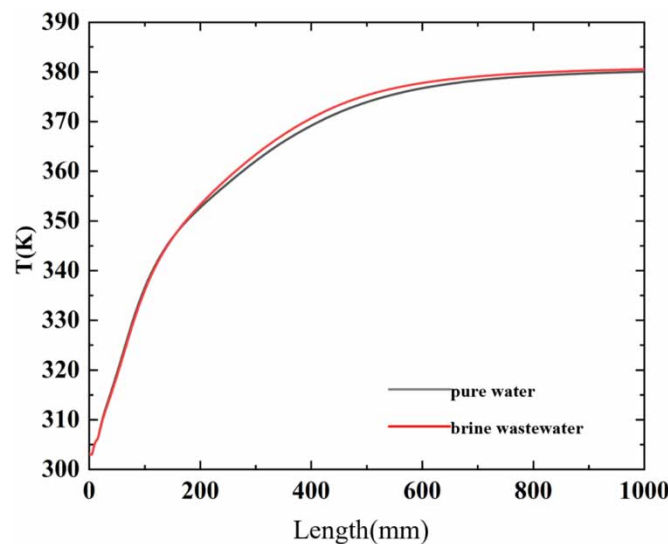

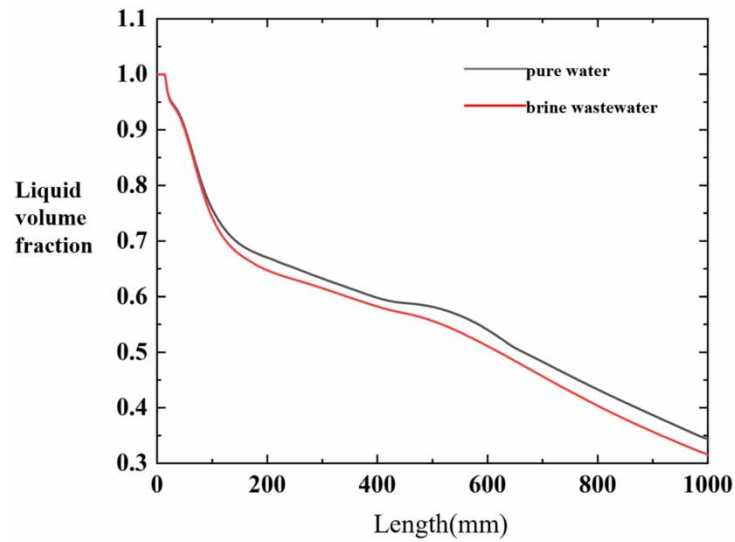**Figure 7** | Axial distribution of the liquid film temperature in the tube.

Figure 8 | Axial distribution of liquid volume fraction of the liquid film in the evaporation tube.

minimum value of about 0.33 at the outlet. Within the range, the liquid volume fraction of the liquid membrane of saline wastewater is slightly smaller than that of the pure water liquid membrane. Combining with the temperature distribution in Figure 6, it can be observed that due to the salt-containing wastewater having better thermal conductivity and lower specific heat capacity, the temperature of the liquid film is higher, which makes the evaporation process proceed faster, so the liquid volume fraction of the salt-containing wastewater liquid film is smaller.

3.2.4. Tangential velocity distribution of saline wastewater and pure water in a vertical tube along the inner wall of the tube

Figure 9 shows the tangential velocity distribution of the saline wastewater and pure water in the vertical pipe along the inner wall of the pipe. It can be established from the figure that the tangential velocity of the liquid film decreases rapidly in the range from 0 to 100 mm from the inlet, and decreases to about 0.18 m/s at 100 mm. While in the range of 100–600 mm, the tangential velocity gradually decreases to 0. Although the simulated saline wastewater has more salt (2% NaCl) than pure water, the
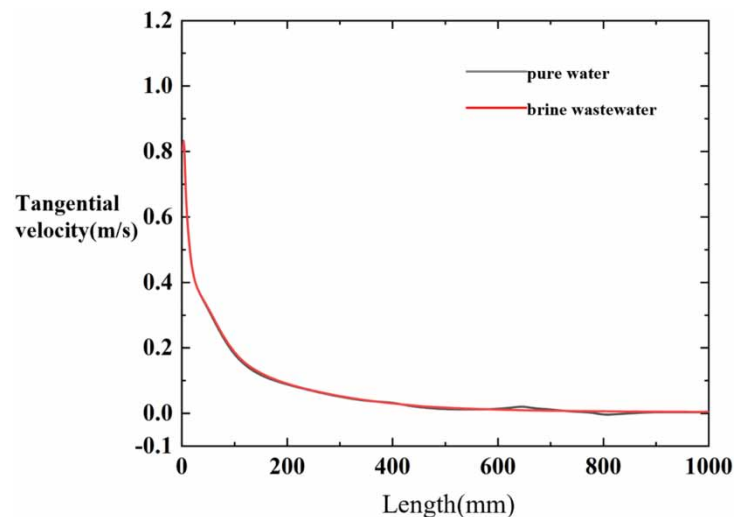

Figure 9 | Axial distribution of tangential velocity of the liquid film in the evaporation tube.

difference in viscosity between the two is smaller than that in Figure 6(d), so the effect on the liquid film velocity is smaller, which makes the difference between the tangential velocity of the liquid film of saline wastewater and that of pure water smaller.

4. CONCLUSION

In this paper, the VOF turbulence model and the RNG k–ε model are utilized to numerically simulate the flow in a vertical falling film evaporation tube with saline wastewater under certain structural parameters and different operating parameters. In addition, the differences in heat and mass transfer between saline wastewater and pure water in a falling film evaporation tube were compared. The main conclusions are as follows:

- The fluid velocity in the tangential inlet vertical tube is greater than that in the vertical inlet vertical tube, and the difference is 0.1 m/s at the vapor–liquid intersection, which makes its heat transfer effect better.
- Compared with the vertical inlet vertical pipe, the tangential inlet vertical pipe fluid turbulence intensity is greater, especially at the vapor–liquid interface, the average difference is about 5%, and the larger turbulence intensity difference is more conducive to the evaporation of liquid film in the pipe.
- The fluid temperature in the vertical tube under the tangential inlet is higher, with a difference of 10 K or less, which leads to higher evaporation efficiency.
- Since the specific heat capacity of saline wastewater is smaller and the thermal conductivity is greater, the liquid film temperature is higher than that of pure water in the range of 193–1,000 mm from the inlet, which results in better heat transfer.
- The liquid volume fraction of saline wastewater is about 0.05 smaller than the volume fraction of pure water liquid membrane, so that the evaporation effect of saline wastewater is better than that of pure water by the falling membrane.

DATA AVAILABILITY STATEMENT

All relevant data are included in the paper or its Supplementary Information.

CONFLICT OF INTEREST

The authors declare there is no conflict.

REFERENCES

Al-Sahali, M. & Ettouney, H. 2007 Developments in thermal desalination processes: design, energy, and costing aspects. *Desalination* **214** (1–3), 227–240.

Bing, L., Youle, L., Chuan, C., Jianliang, X., Huashan, L. & Zhun, M. 2021 Distribution of heat transfer coefficient in the vertical tube of falling film evaporator treating saline wastewater based on micro flow and experimental verification. *Journal of Water Reuse and Desalination* **11** (3), 439–452.

Cao, J., Ren, Y., Zhu, Q. & Ma, Y. 2019 Investigation of solid–liquid equilibria on the $Na^+//Cl^-$, NO_3^-, SO_4^{2-}-H_2O system and the $Na^+//NO_3^-$, SO_4^{2-}-H_2O system at 313.15 K. *Journal of Chemical & Engineering Data* **64** (3), 1209–1221.

Dolatabadi, M., Swiergosz, T. & Ahmadzadeh, S. 2021 Electro-Fenton approach in oxidative degradation of dimethyl phthalate – The treatment of aqueous leachate from landfills. *Science of the Total Environment* **772**, 145323.

Fang, J., Li, K. X. & Diao, M. Y. 2019 Establishment of the falling film evaporation model and correlation of the overall heat transfer coefficient. *Royal Society Open Science* **6** (5), 190135.

Gommed, K., Grossman, G. & Koenig, M. S. 2001 Numerical study of absorption in a laminar falling film of ammonia-water. *The Technical Voice of the Industry* **107**, 452–462.

Karimi, G. & Kawaji, M. 1999 Flow characteristics and circulatory motion in wavy falling films with and without counter-current gas ow. *International Journal of Multiphase Flow* **25**, 1305–1319.

Lappalainen, J., Korvola, T. & Alopaeus, V. 2017 Modelling and dynamic simulation of a large MSF plant using local phase equilibrium and simultaneous mass, momentum, and energy solver. *Computers & Chemical Engineering* **97**, 242–258.

Lefebvre, O. & Moletta, R. 2006 Treatment of organic pollution in industrial saline wastewater: a literature review. *Water Research* **40** (20), 3671–3682.

Li, C., Zhao, R. C., Li, L. & Li, J. M. 2017 Mass transfer characteristics of the high temperature falling film evaporation over a vertical wall under countercurrent laminar airflow. *Experimental Thermal and Fluid Science* **82**, 269–275.

Liu, B., Wang, X., Liu, Y., Gao, Y., Ma, Z. & Xue, J. 2020 Simulation analysis of flow velocity and liquid film of saline wastewater in falling film evaporation. *Environmental Technology & Innovation* **19**, 100790.

Mura, E. & Gourdon, M. 2016 Interfacial shear stress, heat transfer and bubble appearance in falling film evaporation. *Experimental Thermal and Fluid Science* **79**, 57–64.

Ng, K. C., Thu, K., Oh, S. J., Ang, L., Shahzad, M. W. & Ismail, A. B. 2015 Recent developments in thermally-driven seawater desalination: energy efficiency improvement by hybridization of the MED and AD cycles. *Desalination* **356**, 255–270.

Oubella, M., Feddaoui, M. & Mir, R. 2015 Numerical study of heat and mass transfer during evaporation of a thin liquid film. *Thermal Science* **19** (5), 1805–1819.

Shi, J., Huang, W., Han, H. & Xu, C. 2020 Review on treatment technology of salt wastewater in coal chemical industry of China. *Desalination* **493**, 114640.

Tian, Y., Chen, Z., Wang, N., Zhou, D. & Cheng, L. 2018 Numerical and experimental investigation of pool boiling on a vertical tube in a confined space. *International Journal of Heat and Mass Transfer* **122**, 1239–1254.

Wang, W. S., Liao, Y. H., Yan, Y. Z., Zhao, B. C., Wang, T. & Shangguan, S. S. 2020 Numerical study on falling film flowing characteristics of r113 inside vertical tube under different structural conditions. *Chinese Journal of Chemical Engineering* **28** (1), 23–32.

Zezhong, Z. Q. T. L. G. Z. L. 2014 Study on change law of physical-chemical parameters in evaporation of deammoniation waste liquor. *Inorganic Chemicals Industry* **46** (9), 66–78.

Zhang, Y. H., Lu, D. G., Du, Z., Fu, X. L. & Wu, G. H. 2015 Numerical and experimental investigation on the transient heat transfer characteristics of C-shape rod bundles used in Passive Residual Heat Removal Heat Exchangers. *Annals of Nuclear Energy* **83**, 147–160.

Zhang, K., Wen, Z. & Xhang, X. 2002 China's water environment at the beginning of the 21st century: challenges and countermeasures. *Water Science and Technology : A Journal of the International Association on Water Pollution Research* **46** (11–12), 245–251.

Zhao, D., Lun, W. & Wei, J. 2017 Discussion on wastewater treatment process of coal chemical industry. *IOP Conference Series: Earth and Environmental Science* **100**, 012067.

Zhou, S. H., Gong, L. Y., Liu, X. Y. & Shen, S. Q. 2019 Mathematical modeling and performance analysis for multi-effect evaporation/multi-effect evaporation with thermal vapor compression desalination system. *Applied Thermal Engineering* **159**, 113759.